# Channel characterization at 120 GHz for future indoor communication systems*

Chen Zhen(陈 镇) and Cao Jun-Cheng(曹俊诚)†

*Key Laboratory of Terahertz Solid-State Technology, Shanghai Institute of Microsystem and Information Technology, Chinese Academy of Sciences, Shanghai* 200050, *China*

(Received 15 August 2012; revised manuscript received 6 November 2012)

We present a simulation on the spatial and temporal characteristics of the indoor propagation channel at 120 GHz. The simulation, applied to a dynamic scenario with randomly placed objects and moving people in a room, is based on a three-dimensional ray-tracing method. Propagation and reflection mechanisms of electromagnetic waves are discussed in the channel model. The received power in a 0.95-m-height plane is obtained. Comparison between walls and ceiling covered with dielectric mirrors and those with three common wall and ceiling materials are presented. The result shows that the holistic received power level with dielectric mirrors is about 10 dB higher than with other materials.

**Keywords:** sub-terahertz communication, channel models, ray tracing, electromagnetic propagation

**PACS:** 92.60.Ta, 01.20.+x, 87.16.A– **DOI:** 10.1088/1674-1056/22/5/059201

## 1. Introduction

With the demand for higher data rates and mobility, there has been an unprecedented growth in the development and deployment of wireless communication systems. For fast transmission of huge amounts of data with data rates beyond 10 Gbit/s as needed for new emerging applications,[1] the traditional wireless communication systems are hard to support, even though the advanced modulation schemes and signal processing technologies are used to enhance the spectral efficiency. The employment of higher carrier frequencies will be a practical choice. In this approach, even a simple modulation scheme could handle those high data rates.[2] The devices and systems working at these higher carrier frequencies are under development.[3,4] Today, we are at the dawn of a new age of wireless communication systems that operate at terahertz (THz) and sub-terahertz frequencies.

Several companies, including SiBEAM, LG, IBM, and Sony, have products under development operating at 60 GHz.[5] Besides, there are various standards that are under way for 60-GHz wireless local area networks/wireless personal area networks (WLAN/WPAN) applications, such as IEEE 802.15.3c, IEEE 802.11ad, WirelessHD, the WiGig standard, and ECMA 387. In the adjacent sub-terahertz and terahertz range, many efforts have been made. In the 120-GHz band, the NTT group in Japan has developed three types of systems,[6–8] i.e., (i) photonic MMW/UTC-PD sub-THz sources and Schottky diode detectors, (ii) photonic MMW/UTC-PD sub-THz sources and MMIC receivers, and (iii) an integrated MMIC transmitter and receiver. Among these, the all-electronics-based 120-GHz-band system using InP HEMT MMICs was successfully deployed for the broadcasting of HDTV in the 2008 Olympic Games held in Beijing, and for the error-free transmission at 10 Gbit/s. The NTT group focuses on hardware components, while the researchers at Braunschweig Technical University in Germany pay more attention to system modeling.[9,10] They have developed an integrated simulation environment for the investigation of future indoor communication systems operating at frequencies beyond 300 GHz. Through it, the system parameters can be estimated under realistic hardware and propagation conditions.

In contrast with other frequency bands in sub-THz and THz range, the devices operating at 120 GHz may be prevalent at first. According to the propagation properties in this frequency band, besides the applications in outdoor communications as the NTT group has demonstrated, it would also be used for short-range communications, like in indoor environments. Meanwhile, the worldwide available part of the spectrum at around 120 GHz for mobile applications has not been identified yet.[11] In the near future, high speed data transmission will be used, and the understanding of the channel characteristics at 120 GHz for future indoor communication systems is very necessary.

The rest of the paper is organized as follows. Firstly, the propagation and reflection mechanisms of sub-THz/THz waves are discussed, and some results are obtained. Then, the ray-tracing method and the simulation scenario are introduced.

*Project supported by the National High Technology Research and Development Program of China (Grant No. 2011AA010205), the National Natural Science Foundation of China (Grant Nos. 61131006 and 61021064), the Major National Development Project of Scientific Instrument and Equipment, China (Grant No. 2011YQ150021), the Important National Science and Technology Specific Projects, China (Grant No. 2011ZX02707), the Major Project, China (Grant No. YYYJ-1123-1), the International Collaboration and Innovation Program on High Mobility Materials Engineering of the Chinese Academy of Sciences, and the Shanghai Municipal Commission of Science and Technology, China (Grant No. 10JC1417000).

†Corresponding author. E-mail: jccao@mail.sim.ac.cn

© 2013 Chinese Physical Society and IOP Publishing Ltd 

After then, the simulation results are presented. Finally, the conclusions are made.

## 2. Propagation

In the indoor environment, when propagating, sub-THz/THz waves suffer from free space path loss, as well as from atmospheric attenuation (mainly due to gaseous absorption of water vapour and oxygen). The free space path loss can be quantitatively described by the Friis transmission equation, which sets the received signal power $P_{\rm r}$ as

$$P_{\rm r}(d) = \frac{P_{\rm t}G_{\rm t}G_{\rm r}\lambda^2}{(4\pi)^2 d^2}, \tag{1}$$

where $G_{\rm t}$ and $G_{\rm r}$ are Tx and Rx antennas gains, respectively; $P_{\rm t}$ is the transmitted power; $d$ is the distance between the antennas; and $\lambda$ is the wavelength. The atmospheric attenuation is described by $P_{\rm r}(d) = P_{\rm t}\exp(-\alpha d)$, where $\alpha$ is the attenuation coefficient. For a 10-m communication link of 120 GHz, using unity gain antennas, the free-space path loss is about 94.02 dB, while the atmospheric attenuation is very low ($< 0.05$ dB),[9] due to the short distance and the good atmospheric condition in the indoor environment. Therefore, the attenuation of 120-GHz waves is mainly determined by free-space path loss.

## 3. Reflection

Apart from free space path loss and atmospheric attenuation, sub-THz/THz waves also suffer from reflections and scatterings of objects in propagation. Thus, the effects of object surfaces on the propagation of sub-THz/THz waves need to be understood for designing proper indoor wireless communication systems. In this paper, we consider three different reflection mechanisms. They are the models for reflections from optically thick smooth single-layer materials,[12] for diffuse reflections in specular direction from optically thick rough single-layer materials,[13] and for reflections from optically thin smooth multi-layer materials.[14]

(i) For reflections from optically thick smooth single-layer materials, the reflection coefficient can be calculated using classical Fresnel equations as

$$r_{\rm TE} = \frac{\tilde{n}_1\cos\theta_1 - \tilde{n}_2\cos\theta_2}{\tilde{n}_1\cos\theta_1 + \tilde{n}_2\cos\theta_2}, \quad r_{\rm TM} = \frac{\tilde{n}_2\cos\theta_1 - \tilde{n}_1\cos\theta_2}{\tilde{n}_2\cos\theta_1 + \tilde{n}_1\cos\theta_2}. \tag{2}$$

Here, $\theta_1$ is the angle of incidence and also the angle of reflection, $\theta_2 = \arcsin(\sin\theta_1(\tilde{n}_1/\tilde{n}_2))$ the angle of refraction, $\tilde{n}_1$ the free space index of refraction which equals 1, and $\tilde{n}_2$ the complex index of refraction of the reflecting material. The value of $\tilde{n}_2$ can be obtained by $\tilde{n}_2 = n_2(1+{\rm i}\kappa)$, where $n_2$ is the index of refraction, $\kappa = \alpha c/(4\pi f n_2)$ is the extinction coefficient, $\alpha$ is the absorption coefficient, and $c$ is the speed of light in a vacuum.

(ii) For diffuse reflections in specular direction from optically thick rough single-layer materials, the Fresnel reflection coefficient must be multiplied by the Rayleigh roughness factor $\rho$. That is, $r'_{\rm TE} = \rho r_{\rm TE}$ and $r'_{\rm TM} = \rho r_{\rm TM}$, where $\rho = \exp(-g/2)$, with $g = (4\pi f\cdot\sigma\cdot\cos\theta_1/c)^2$. Here, $\sigma$ is the standard deviation of the surface roughness.

(iii) For reflections from optically thin smooth multi-layer materials, the transfer matrix method can be used to calculate the reflection coefficient. The behavior of a propagating wave in a multilayer material can be described by

$$\begin{aligned}\begin{pmatrix} E_{\rm inc} \\ E_{\rm ref}\end{pmatrix} &= I_0\left(\prod_{m=1}^{N}\boldsymbol{P}_m\boldsymbol{I}_m\right)\begin{pmatrix} E_{\rm trans} \\ 0\end{pmatrix} \\ &= \begin{pmatrix} a_{11}a_{12} \\ a_{21}a_{22}\end{pmatrix}\begin{pmatrix} E_{\rm trans} \\ 0\end{pmatrix} = \begin{pmatrix} a_{11} \\ a_{21}\end{pmatrix}E_{\rm trans},\end{aligned} \tag{3}$$

where $E_{\rm inc}$ is the incident field, $E_{\rm ref}$ the reflective field, and $E_{\rm trans}$ the transmitted field, and

$$\boldsymbol{P}_m = \begin{pmatrix} {\rm e}^{-{\rm i}\tilde{n}_m k_0\cos\theta_m l_m} & 0 \\ 0 & {\rm e}^{{\rm i}\tilde{n}_m k_0\cos\theta_m l_m}\end{pmatrix},$$
$$\boldsymbol{I}_m = \frac{1}{t_{\rm TE/TM}}\begin{pmatrix} 1 & r_{\rm TE/TM} \\ r_{\rm TE/TM} & 1\end{pmatrix},$$

with $\tilde{n}_m$ being the complex refractive index, $k_0$ the wave number in free space, $\theta_m$ the angle of propagation, and $l_m$ the thickness of layer $m$. Here,

$$r_{\rm TE} = \frac{\tilde{n}_m\cos(\theta_m) - \tilde{n}_{m+1}\cos(\theta_{m+1})}{\tilde{n}_m\cos(\theta_m) + \tilde{n}_{m+1}\cos(\theta_{m+1})},$$
$$t_{\rm TE} = \frac{2\tilde{n}_m\cos(\theta_m)}{\tilde{n}_m\cos(\theta_m) + \tilde{n}_{m+1}\cos(\theta_{m+1})},$$
$$r_{\rm TM} = \frac{\tilde{n}_{m+1}\cos(\theta_m) - \tilde{n}_m\cos(\theta_{m+1})}{\tilde{n}_{m+1}\cos(\theta_m) + \tilde{n}_m\cos(\theta_{m+1})},$$
$$t_{\rm TM} = \frac{2\tilde{n}_m\cos(\theta_m)}{\tilde{n}_{m+1}\cos(\theta_m) + \tilde{n}_m\cos(\theta_{m+1})},$$

which are the classical Fresnel equations. The reflection coefficient can be obtained by $r = E_{\rm ref}/E_{\rm inc} = a_{21}/a_{11}$.

We list the parameters of eight different materials which are commonly used in daily life, in Table 1.[15] It is needed to add that for plaster covered with white paint, the white paint layer has a thickness of 0.695 mm, a refractive index of 2.09 and an absorption coefficient of 2 cm$^{-1}$; the plaster layer has a refractive index of 1.61 and an absorption coefficient of 0.8 cm$^{-1}$. For double pane glass window, it consists of a 2.92-mm-thick glass layer, a 1.96-mm-thick air layer and then again a 2.92-mm-thick glass layer. The refractive index and the absorption coefficient of both the glass layers are 2.56 cm$^{-1}$ and 3 cm$^{-1}$, respectively. Then, we simulate the absolute values of the reflection coefficients of these materials at 120 GHz. The results are shown in Fig. 1.

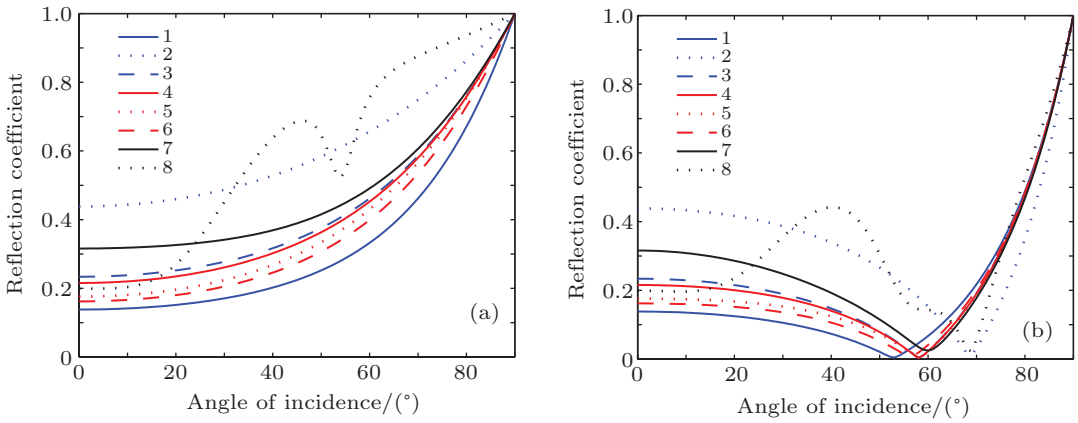



**Fig. 1.** (color online) Simulated absolute values of the reflection coefficients for (a) TE and (b) TM polarizations of 8 materials with 3 different mechanisms.

**Table 1.** Parameters of eight different materials.

| No. | Material | Mechanism | Refractive index | Absorption coefficient/cm$^{-1}$ | Standard deviation/mm |
|---|---|---|---|---|---|
| 1 | Wood | A | 1.32 | 1.25 | 0 |
| 2 | Glass | A | 2.56 | 3 | 0 |
| 3 | Plaster | A | 1.61 | 0.8 | 0 |
| 4 | Plaster1 | B | 1.61 | 0.8 | 0.05 |
| 5 | Plaster2 | B | 1.61 | 0.8 | 0.15 |
| 6 | Wallpaper | B | 1.5 | 2 | 0.13 |
| 7 | Plaster covered with white paint | C | 2.09 | 2 | 0 |
| | | | 1.61 | 0.8 | 0 |
| 8 | Double pane glass window | C | 2.56 | 3 | 0 |

## 4. Ray tracing

Ray tracing is a deterministic tool based on geometrical optics for investigating the properties of wireless communication channels. It provides extremely accurate site-specific propagation coverage models that can be used for practical system deployment.[16] Such site-specific methods are supposed to be even more accurate as carrier frequencies fall into the sub-THz/THz regime. In our simulations, ray-tracing is adopted, and implemented with the image method.[17]

The simulation scenario for sub-THz cells is an office room with dimensions of 6 m×5 m×2.5 m, as shown in Fig. 2. There are windows and a door in their corresponding wall, and closets against the wall and a picture frame on the wall, while other parts of the walls are covered with flexible omni-directional dielectric mirrors.[18,19] It is assumed that the reflection coefficient for each of these mirrors is independent of angle and equals 0.93 for both TE and TM polarizations. A few pieces of furniture are placed in the room, including a table, a sofa, a bookcase, and a cabinet. Three persons are walking randomly in the room with a maximum speed of 0.5 m/s, keeping a distance of at least 1 m from each other. The transmitter with an available output power of 10 dBm[20] is suspended from the ceiling in the middle of the room, and at a height of 2.3 m above the floor, i.e., at the position of ($x = 3$ m, $y = 2.5$ m, $z = 2.3$ m), with the origin located in the bottom left corner. The position of the receiver varies on a 57×47 grid which keeps a 0.2-m offset from the walls, in the plane $z = 0.95$ m above the floor, corresponding to the height of a possible location of a sub-THz communication device on the desktop. The gains of both Tx and Rx antennas are set to be 20 dBi with a horn antenna type, according to Ref. [20]. The Tx and Rx antennas are assumed to be aligned directly or indirectly through reflections in the specular directions through a tracking system which dynamically chooses the best possible single path, either line-of-sight

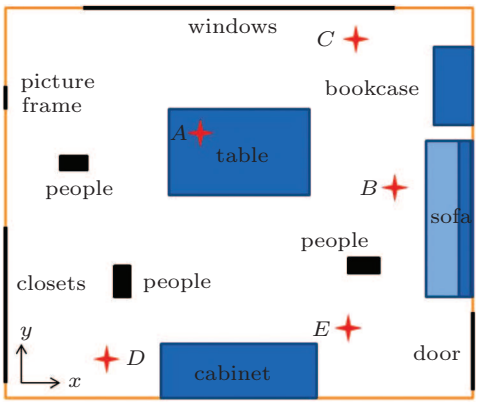



**Fig. 2.** (color online) Floor plan of the simulation scenario.

(LOS) or non-line-of-sight (NLOS). Therefore, there is a single propagation path at a time. The multipath effect caused by the antenna side lobes[21] and incoherent diffuse scattering is neglected in the current version.

Between the fixed Tx and the Rx which is randomly placed in the receiving plane, we consider three kinds of propagation paths: LOS path, once-reflected paths, and twice-reflected paths. The reflections rely on the walls and ceiling. The reflections from the floor are not taken into account as they are assumed to be absorbed by the carpet or blocked, for example, by the table that the receiver device is placed on. For each path, besides the attenuation caused by the propagation and the reflection, there is an additional insertion loss of 55 dB[22,23] if it happens to be crossed by moving people or other objects. This means that once a path is blocked, the received power through it would be below the receiving sensitivity level which we set as $-50$ dBm, while in Ref. [20] the theoretical sensitivity level for a BER of $10^{-12}$ is $-44.7$ dBm when G.709 FEC is used.

## 5. Simulation results

First, we simulate the received power for TE polarization in the receiving plane at a random time point as shown in Fig. 3. In this scenario, three people stand randomly in the room. The white areas in the receiving plane are 0.2 m offset from the walls, or furniture and people where a receiver cannot be placed, aiming to increase the resolution of the color range. The table and sofa are 0.9 m and 0.35 m high, respectively. Thus, they are under the receiving plane and not shown in the figure. We can see in Fig. 3(a) that the LOS path exists in most areas, and contributes to a considerable received power of above $-40$ dBm. However, in some corners and the areas behind persons, the LOS path is blocked by furniture or people, and the received power drops to below $-90$ dBm. For once-reflected paths shown in Fig. 3(b), the holistic received power level turns lower, but some of the shadowing areas in Fig. 3(a) disappear. Still, the lowest received power is around $-90$ dBm. Through the distribution, we know that the reflection from the ceiling is relied on mostly, as the distance through it from the transmitter to the respective receiver is the shortest in all possible paths. For twice-reflected paths, the holistic received level becomes even lower, and the distribution changes. The received power does not decrease from the centre of the room towards the walls any more. But there is no blocked path, and the lowest received power is higher than $-48$ dBm. We obtain the strongest received signal from direct, once- and twice-reflected propagation paths as the final received signal, which is shown in Fig. 3(d). Since for most areas in the receiving plane the final received power is determined by LOS path or once-reflected path through the ceiling, the special areas on the walls (windows, closets, the picture frame, and the door) have very little influence on the received power level.

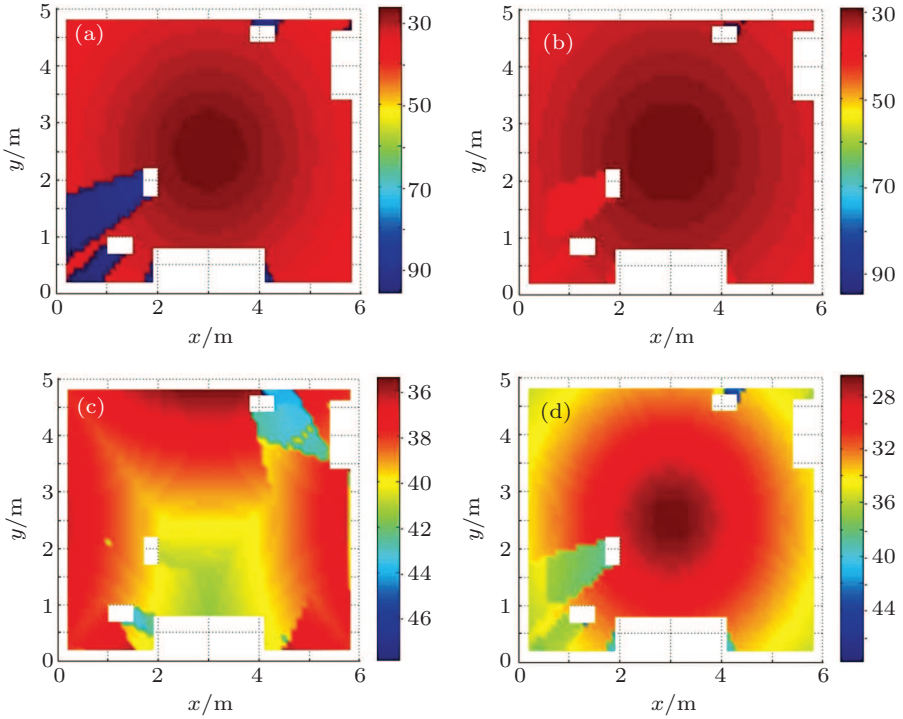



**Fig. 3.** (color online) Values of the received power (in dBm) by (a) LOS path, (b) once-reflected path, and (c) twice-reflected path in the receiving plane. (d) Value of the final received power in the receiving plane.

Then we make the three people start to walk randomly, and obtain the final received power at several fixed positions ($A$, $B$, $C$) and randomly moving positions ($D$, $E$) in the receiving plane, as shown in Fig. 4. We can see that, for Rx position A, the received power is the highest and invariable, because of its LOS path, which is shortest and can hardly be blocked. For Rx positions $B$ and $C$, the received power is lower, and it sometimes drops off when the LOS path is blocked and NLOS paths take place. For the moving Rx positions $D$ and $E$, the received power varies, and sometimes drops to below $-50$ dBm when the LOS and NLOS paths are both blocked, as we expected. We could know that for an either fixed or moving Rx, the received power is considerable in most of the time passing through LOS or NLOS paths; it seldom falls below the receiving sensitivity, when all the paths are blocked. For a general understanding of the temporal characteristics, we also obtain the worst-case received signal power of the receiving plane in Fig. 5. The crimson area in the center of the room is due to the arrangement of the table. The blue areas which represent the shadowed areas are located near the furniture. Obviously, these areas would become larger when the simulation time becomes longer. Still, in these areas the probability for them to be shadowed is extremely low ($< 0.5\%$). This shows that the NLOS paths are a forceful guarantee for a high degree of robustness against shadowing.

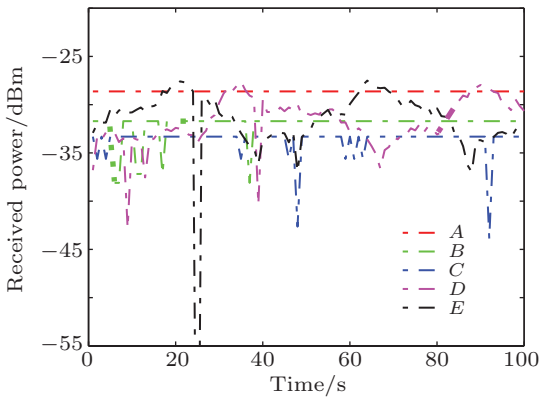



**Fig. 4.** (color online) Received power at the receiving positions varying with time.

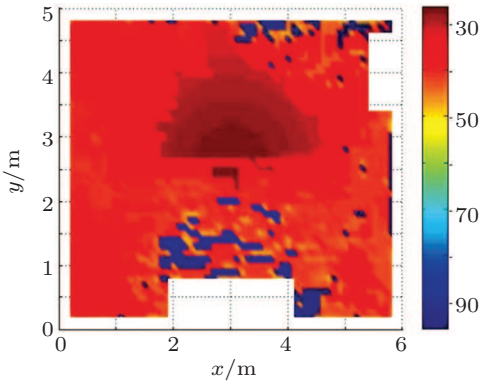



**Fig. 5.** (color online) The worst case of received power (in dBm) in the receiving plane.

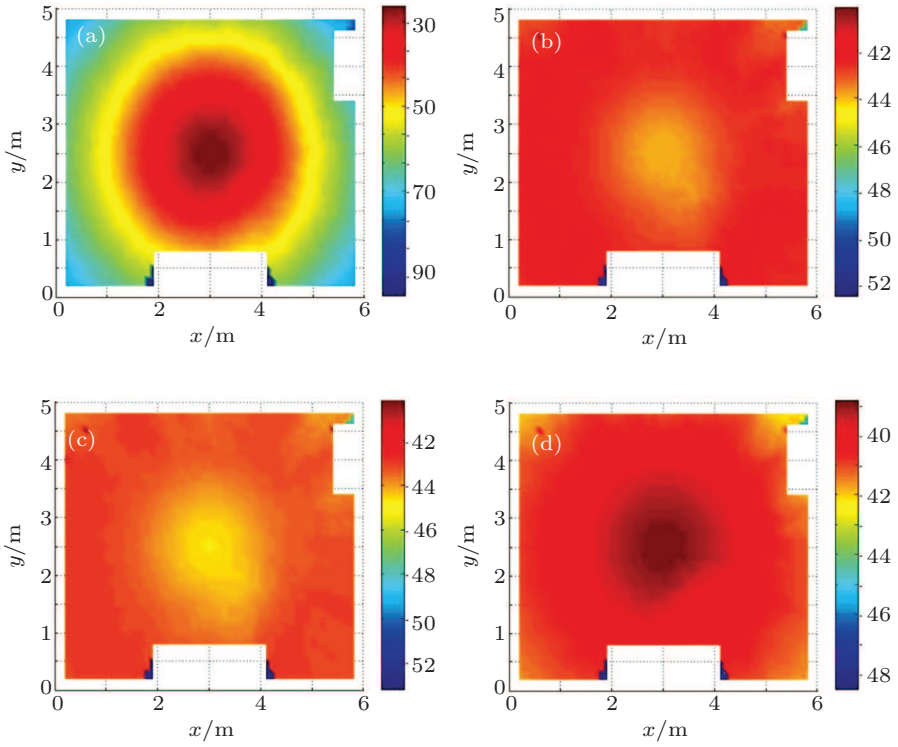



**Fig. 6.** (color online) Mean values of received power (in dBm) of the NLOS paths for TE polarization with (a) dielectric mirrors, (b) wallpaper, (c) plaster, and (d) plaster covered with white paint.

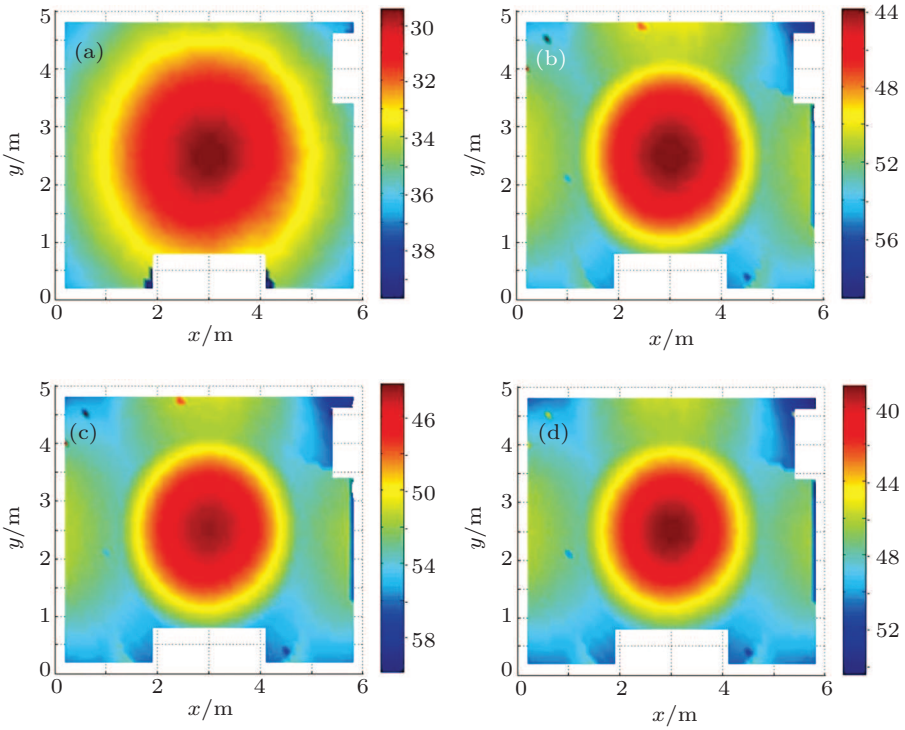



**Fig. 7.** (color online) Mean values of received power (in dBm) of the NLOS paths for TM polarization with (a) dielectric mirrors, (b) wallpaper, (c) plaster, and (d) plaster covered with white paint.

For most receiving positions in most of the time, the link depends on the LOS path. But the lowest received power level for each Rx position is determined by the NLOS paths. Thus we obtain the mean values of received power of NLOS paths in a 100 s time range. The strongest received power from once- and twice-reflected propagation paths is chosen for each Rx position all the time. Meanwhile, in order to study the influences of different wall and ceiling materials, we replace the dielectric mirrors with plaster with a 0.15-mm standard deviation of the surface roughness (No. 5 in Table 1), common wallpaper (No. 6 in Table 1), and plaster covered with white paint (No. 7 in Table 1) separately. The results are shown in Fig. 6 for TE polarization and in Fig. 7 for TM polarization. We can see that for TE polarization in Fig. 6, the holistic received power level with dielectric mirrors is about 10 dB higher than with the others. For dielectric mirrors and plaster covered with white paint, the received power each decreases from the centre of the room towards the walls, while for plaster and wallpaper, the received power increases. This is the result of competition between propagation path length and reflection angle, of which the reflection coefficients are different from each other for different materials. The results and reason are very similar to the situations in Ref. [13]. For both TE and TM polarizations, the received power levels for plaster covered with white paint, are a little higher than for common wallpaper or plaster.

## 6. Conclusion

In this article, we discuss the propagation mechanism and three reflection models of 120-GHz waves, and obtain the reflection coefficients of several common materials. The ray-tracing method and the simulation scenario are introduced. We simulate the spatial and temporal characteristics of the indoor propagation channel at 120 GHz, and obtain the values of the received power in the receiving plane. The result shows that the link by LOS path is not robust, for it can be broken by moving people or other objects. For a high degree of robustness against shadowing, the NLOS paths should be applied. With dielectric mirrors covering the walls and ceiling, the holistic received power level is about 10 dB higher than with some other common building materials. Thus the dielectric mirrors are necessary when the transmitted power or the antenna gain is not high enough, or the receiving sensitivity is very low. Our next work will deal with the transmission attenuations of materials like wood, and the diffuse scattering from rough surfaces.

## Acknowledgement

The authors would like to thank Dr. X. G. Guo, Dr. H. Li, and Dr. R. Zhang for helpful discussion and suggestions, and careful reading of this manuscript.

## References

[1] Cherry S 2004 *IEEE Spectrum* **41** 58

[2] Barbieri S, Maineult W, Dhillon S S, Sirtori C, Alton J, Breuil N, Beere H E and Ritchie D A 2007 *Appl. Phys. Lett.* **91** 143510

[3] John F and Lothar M 2010 *J. Appl. Phys.* **107** 111101

[4] Shi Y L, Zhou Q L and Zhang C L 2009 *Chin. Phys. B* **18** 5511

[5] Rappaport T S, Murdock J N and Gutierrez F 2011 *Proc. IEEE* **99** 1390

[6] Hirata A, Kosugi T, Meisl N, Shibata T and Nagatsuma T 2004 *IEEE Trans. Microw. Theory* **52** 1843

[7] Hirata A, Takahashi H, Yamaguchi R, Kosugi T, Murata K, Nagatsuma T, Kukutsu N and Kado Y 2008 *J. Lightwave Technol.* **26** 2338

[8] Takahashi H, Kosugi T, Hirata A, Murata K and Kukutsu N 2010 *IEEE Trans. Microw. Theory* **58** 4072

[9] Piesiewicz R, Kleine-Ostmann T, Krumbholz N, Mittleman D, Koch M, Schoebel J and Kürner T 2007 *IEEE Antennas Propag. Mag.* **49** 24

[10] Kürner T, Jacob M, Piesiewicz R and Schoebel J 2008 *Simul.-T. Soc. Mod. Sim.* **84** 123

[11] Jacob M, Priebe S, Kürner T, Jastrow C, Kleine-Ostmann T and Schrader T *2009 IEEE GLOBECOM Workshops*, November 30–December 4, 2009 Honolulu, Hawaii, USA, p. 435

[12] Piesiewicz R, Kleine-Ostmann T, Krumbholz N, Mittleman D, Koch M and Kürner T 2005 *Electron. Lett.* **41** 1002

[13] Piesiewicz R, Jansen C, Mittleman D, Kleine-Ostmann T, Koch M and Kürner T 2007 *IEEE Trans. Antennas Propag.* **55** 3002

[14] Jansen C, Piesiewicz R, Mittleman D, Kürner T and Koch M 2008 *IEEE Trans. Antennas Propag.* **56** 1413

[15] Piesiewicz R, Jansen C, Wietzke S, Mittleman D, Koch M and Kürner T 2007 *Int. J. Infrared Milli. Waves* **28** 363

[16] Rappaport T S 1996 *Wireless Communications: Principles and Practice* (Prentice-Hall) pp. 235–241

[17] Sarkar T K, Ji Z, Kim K, Medouri A and Salazar-Palma M 2003 *IEEE Antennas Propag. Mag.* **45** 51

[18] Krumbholz N, Gerlach K, Rutz F, Koch M, Piesiewicz R and Kürner T 2006 *Appl. Phys. Lett.* **88** 202905

[19] Zhang R, Li H, Cao J C and Feng S L 2009 *Acta Phys. Sin.* **58** 4618 (in Chinese)

[20] Hirata A, Yamaguchi R, Kosugi T, Takahashi H, Murata K, Nagatsuma T, Kukutsu N, Kado Y, Iai N, Okabe S, Kimura S, Ikegawa H, Nishikawa H, Nakayama T and Inada T 2009 *IEEE Trans. Microw. Theory* **57** 1102

[21] Driessen P F 1996 *IEEE Trans. Commun.* **44** 1034

[22] Piesiewicz R, Jemai J, Koch M and Kürner T 2004 *Joint 29th International Conference on IRMMW and 12th International Conference on Terahertz Electronics*, September 27–October 1, 2004, p. 539

[23] Jacob M, Priebe S, Maltsev A, Lomayev A, Erceg V and Kürner T 2011 *Proceedings of the 5th European Conference on Antennas and Propagation,* April 11–15, 2011, Rome, Italy, p. 3084